

Probabilistic aspects of strength of unidirectional fibre-reinforced composites with matrix failure

HIROSHI SUEMASU

Institute of Interdisciplinary Research, Faculty of Engineering, University of Tokyo, Tokyo, Japan

In the previous paper [1], the stress distribution and the expected number of successive fibre breakages around broken fibres were calculated. It showed the following results. The fracture process that the crack originates from one isolated broken fibre and propagates due to the stress redistribution following the fibre breakage is unlikely to occur in the real unidirectional fibre-reinforced composite material. The matrix-failure is considered to play an important role in the fracture process of real composite materials. In the present paper, the stress (or strain) distribution and the expected number of successive fibre breakages around broken fibres are calculated when the matrix-damaged regions exist. The stress (or strain) distribution is obtained based on the three-dimensional hexagonal-array shear-lag model. Uniform shear force is assumed to occur in the matrix-damaged region. The expected number of the successive fibre breakages is calculated on the assumption that the flaws in the fibre follow a Poisson process.

1. Introduction

Probabilistic aspects of the strength of composite materials have been studied by many workers. Some have paid attention to the scatter in fibre strength and have attempted to understand the behaviour of composite materials from micro-mechanical standpoint. In order to obtain the probability of the fracture stress, they introduced some assumptions to the load redistribution around the broken fibres, for example, ELS (equal load sharing) rule [2] and LLS (local load sharing) rule [3]. However, these assumptions are not realistic and may lead to a fracture pattern that does not occur in the real composite.

In order to clarify this problem, the fracture mechanism was studied based on the more realistic stress model in the previous paper [1]. The stress distribution around broken fibres was calculated on the three-dimensional hexagonal-array shear-lag model [5] and the expected number of successive fibre breakages was obtained on the assumption that fibres break at the flaws which follow a Poisson process in space. It shows that the

expected number of flaws which break due to the stress increase in the neighbouring fibres is very small compared with not only that of LLS rule but also that of the flaws breaking under the initially given uniform strain and presenting within the distance ζ^* in the adjacent fibres. ζ^* is the size of the region of increased stress (or strain) in the neighbouring fibre. Therefore, multiple fibre breakage is essential for the fracture process of real composite. In the present paper, the matrix failure is assumed to occur if the shear force between a broken fibre and its neighbouring one exceeds a certain level. The strain and the expected number of successive fibre breakages are calculated on the same assumption as in the previous paper [1].

2. Theory

2.1. Displacement and strain around broken fibres with matrix failure

Consider an infinite unidirectional fibre-reinforced composite as indicated in Fig. 1. Displacement and strain around broken fibres are analysed on a hexagonal-array shear-lag model when matrix

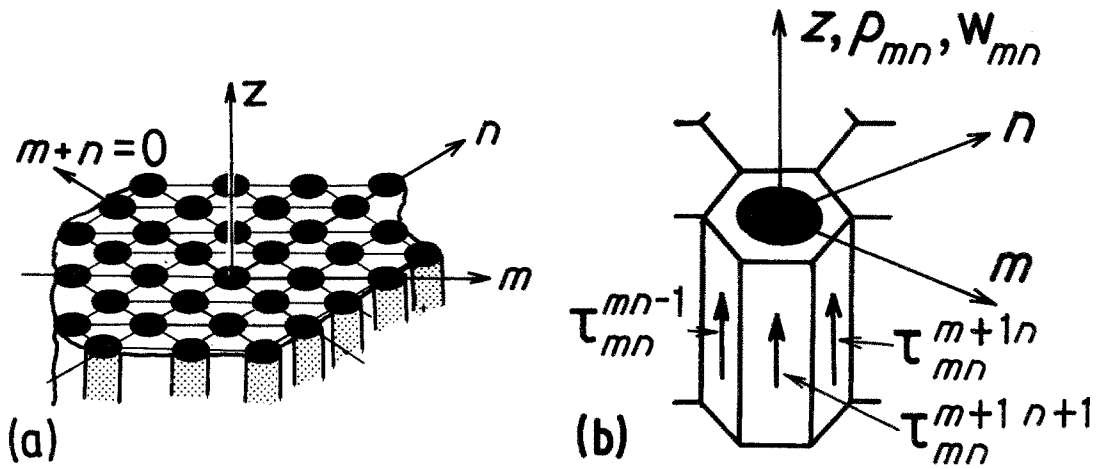


Figure 1 The analytical model; (a) hexagonal-array shear-lag model and its coordinate system. (b) free body diagram as a typical element.

failure exists. Both the fibre and the matrix are assumed to be linear elastic except the matrix-damaged region. The coordinates and a typical element are shown in Fig. 1.

The axial force $p_{mn}(z)$ supported by (m, n) element is assumed to be expressed by using axial displacement $w_{mn}(z)$ of the fibre centre as

$$p_{mn}(z) = E_L A_E \frac{dw_{mn}}{dz} \quad (1)$$

where E_L and A_E are Young's modulus of the composite in the fibre direction and cross-sectional area of an element respectively. Shear force $q_{mn}^{kl}(z)$ between elements (m, n) and (k, l) is assumed to be given as

$$q_{mn}^{kl}(z) = G^*(w_{kl} - w_{mn}) \quad (2)$$

where $G^* [= G_{LT}/(3)^{1/2}]$ is an equivalent shear stiffness and is determined so that the shear modulus of the present model coincides with that of real composite G_{LT} (see [1]). When the (k, l) element is not adjacent to the (m, n) element, q_{mn}^{kl} is zero.

The equilibrium equation of this system is written as

$$\frac{dp_{mn}}{dz} + \sum_{(k,l)}^{(m,n)} q_{mn}^{kl}(z) = f_{mn}(z) \quad (3)$$

where $\sum_{(k,l)}^{(m,n)} q_{mn}^{kl}$ indicates a summation as

$$\sum_{(k,l)}^{(m,n)} q_{mn}^{kl} = q_{mn}^{m+1,n} + q_{mn}^{m-1,n} + q_{mn}^{m,n+1} + q_{mn}^{m,n-1} + q_{mn}^{m+1,n-1} + q_{mn}^{m-1,n+1} \quad (4)$$

and $f_{mn}(z)$ is the term which is induced by the defects (fibre breakages and matrix failure) in the composite [4].

In the matrix-damaged region, the matrix is assumed to support a constant shear force \tilde{q} which is independent of the relative displacement. When the fibres break at the positions $\{(z_j, m_j, n_j); j = 1, 2, \dots, N\}$, f_{mn} is expressed as

$$f_{mn}(z) = \sum_{(k,l)}^{(m,n)} \tilde{Q}_{mn}^{kl}(z) \tilde{I}_{mn}^{kl}(z) + E_L A_E \sum_{j=1}^N \delta_{mm_j} \delta_{nn_j} \frac{d}{dz} \{\tilde{\delta}(z - z_j)\} w_j^0 \quad (5)$$

where

$$\tilde{Q}_{mn}^{kl}(z) = ||| |q_{mn}^{kl}(z)| - \tilde{q} ||| \text{sign} [q_{mn}^{kl}(z)] \quad (6)$$

$$\tilde{w}_j^0 = \frac{1}{2} \lim_{\Delta \rightarrow 0} [w_{m_j n_j}(z_j + \Delta) - w_{m_j n_j}(z_j - \Delta)] \quad (7)$$

$$||| A ||| = \begin{cases} A & A \geq 0 \\ 0 & A < 0 \end{cases}$$

$$\text{sign} A = \begin{cases} 1 & A > 0 \\ 0 & A = 0 \\ -1 & A < 0 \end{cases}$$

$$I_{mn}^{kl}(z) = \begin{cases} 1 & \text{in the matrix-damaged region} \\ 0 & \text{all but above region} \end{cases}$$

$$\delta_{mn} = \begin{cases} 1 & m = n \\ 0 & m \neq n \end{cases}$$

and $\tilde{\delta}(z)$ is Dirac's delta function.

Substituting Equations 1 and 2 into Equation 3, a following difference-differential equation for w_{mn} is obtained:

$$E_L A_E \frac{d^2 w_{mn}}{dz^2} + G^* \sum_{(k,l)}^{(m,n)} (w_{kl} - w_{mn}) = f_{mn} \quad (8)$$

Equation 8 is rewritten in a nondimensional form as

$$\frac{d^2 W_{mn}}{dz^2} + \sum_{(k,l)}^{(m,n)} (W_{kl} - W_{mn}) = F_{mn} \quad (9)$$

where

$$F_{mn}(\xi) = \sum_{(k,l)}^{(m,n)} Q_{mn}^{kl}(\xi) I_{mn}^{kl}(\xi) + \sum_{j=1}^N \delta_{mm_j} \delta_{nn_j} \times \frac{d}{d\xi} \{ \bar{\delta}(\xi - \xi_j) \} W_j^0 \quad (10)$$

$$Q_{mn}^{kl}(\xi) = \bar{Q}_{mn}^{kl}(z) / [\epsilon_\infty (G^* E_L A_E)^{1/2}] \quad (11)$$

$$W_j^0 = \frac{1}{2} \lim_{\Delta \rightarrow 0} \{ W_{mm_j}(\xi_j + \Delta) - W_{m_j n_j}(\xi_j - \Delta) \} \quad (12)$$

$$\xi = \{ [G^* / (E_L A_E)]^{1/2} \} z \quad (13)$$

$$W_{mn}(\xi) = \{ [G^* / (E_L A_E)]^{1/2} / \epsilon_\infty \} w_{mn}(z) \quad (14)$$

$$S_{mn}(\xi) = p_{mn}(z) / (E_L A_E \epsilon_\infty) = dW/d\xi \quad (15)$$

and ϵ_∞ is a strain given at $\xi = \pm \infty$.

Boundary conditions are

$$S_{mn} = 1 \quad \xi = \pm \infty \quad (16)$$

for all fibres, and

$$S_{m_j n_j}(\xi_j) = 0 \quad (17)$$

for broken fibres ($j = 1, 2, \dots, N$).

Instead of solving this problem based on the above boundary conditions as shown in Fig. 2a, a superposition principle is applied as shown in Fig. 2. The solution of Fig. 2b is self-evident and $W_{mn} = \xi$. Therefore, only the solution of Fig. 2c is required to be solved.

Let us introduce auxiliary functions $\tilde{W}(\xi, \theta, \phi)$ and $\tilde{F}(\xi, \theta, \phi)$, which are expressed by $W_{mn}(\xi)$ and $F_{mn}(\xi)$ as

$$\tilde{W}(\xi, \theta, \phi) = \sum_{m=-\infty}^{\infty} \sum_{n=-\infty}^{\infty} W_{mn}(\xi) \times \exp[-i(m\theta + n\phi)] \quad (18)$$

$$\tilde{F}(\xi, \theta, \phi) = \sum_{m=-\infty}^{\infty} \sum_{n=-\infty}^{\infty} F_{mn}(\xi) \times \exp[-i(m\theta + n\phi)] \quad (19)$$

\tilde{W} , W_{mn} and \tilde{F} , F_{mn} are pairs of Fourier transform, respectively, so that W_{mn} and F_{mn} can be

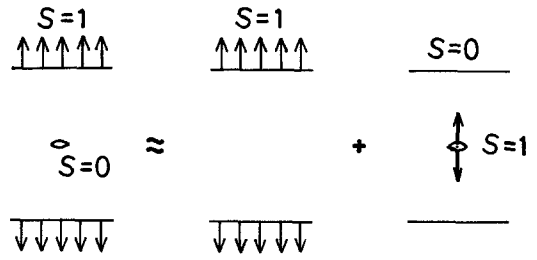


Figure 2 Superposition principle.

expressed by \tilde{W} and \tilde{F} as

$$W_{mn}(\xi) = \left(\frac{1}{2\pi} \right)^2 \int_{-\pi}^{\pi} \int_{-\pi}^{\pi} \tilde{W}(\xi, \theta, \phi) \times \exp[i(m\theta + n\phi)] d\theta d\phi \quad (20)$$

$$F_{mn}(\xi) = \left(\frac{1}{2\pi} \right)^2 \int_{-\pi}^{\pi} \int_{-\pi}^{\pi} \tilde{F}(\xi, \theta, \phi) \times \exp[i(m\theta + n\phi)] d\theta d\phi \quad (21)$$

The matrix failure is assumed to occur only in the regions $|\xi - \xi_j| < \alpha_j$ around the broken fibres as shown in Fig. 3. Substituting Equation 10 into Equation 19, \tilde{F} is written as

$$\tilde{F}(\xi, \theta, \phi) = \sum_{j=1}^N \left(\sum_{(k,l)}^{(m_j, n_j)} Q_{m_j n_j}^{kl}(\xi) U(\alpha_j - |\xi - \xi_j|) \right) \times \{ \exp[i(m_j \theta + n_j \phi)] - \exp[i(k\theta + l\phi)] \} + W_j^0 \left(\frac{d}{d\xi} \bar{\delta}(\xi - \xi_j) \right) \exp[i(m_j \theta + n_j \phi)] \quad (22)$$

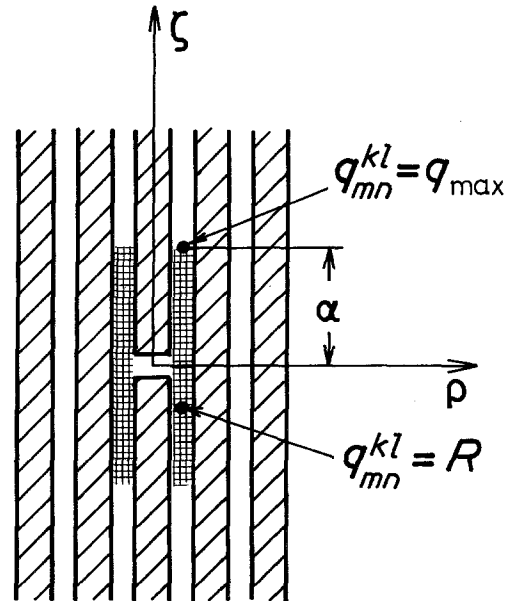


Figure 3 A sketch of matrix damaged region.

where

$$U(\xi) = \begin{cases} 1 & \xi \geq 0 \\ 0 & \xi < 0 \end{cases}$$

Substitution of Equations 20 and 21 into Equation 9 gives

$$\left(\frac{1}{2\pi}\right)^2 \int_{-\pi}^{\pi} \int_{-\pi}^{\pi} \left[\frac{\partial^2 \tilde{W}}{\partial \xi^2} - \lambda^2 \tilde{W} - \tilde{F} \right] \times \exp [i(m\theta + n\phi)] d\theta d\phi = 0 \quad (23)$$

where

$$\lambda(\theta, \phi) = \{2[3 - \cos \theta - \cos \phi - \cos(\theta - \phi)]\}. \quad (24)$$

As Equation 23 holds for any pair of (m, n) , the following equation is obtained:

$$\frac{\partial^2 \tilde{W}}{\partial \xi^2} - \lambda^2 \tilde{W} = \tilde{F}. \quad (25)$$

As \tilde{W} is finite at $\xi = \pm \infty$, the general solution of Equation 25 is written in an integral form as

$$\begin{aligned} \tilde{W}(\xi, \theta, \phi) &= -\frac{1}{2\lambda} \int_{-\infty}^{\infty} \exp[-\lambda|\xi - s|] \\ &\quad \times \tilde{F}(s, \theta, \phi) ds \\ &= \sum_{j=1}^N \{W_j^0 \text{sign}(\xi - \xi_j) \\ &\quad \times \exp[-\lambda|\xi - \xi_j| + i(m_j\theta + n_j\phi)]\} \\ &\quad - \frac{1}{2\lambda} \sum_{(k,l)}^{(m_j, n_j)} \int_{\xi_j - \alpha_j}^{\xi_j + \alpha_j} Q_{m_j n_j}^{kl}(s) \\ &\quad \times \exp[-\lambda|\xi - s|] ds \\ &\quad \times \{\exp[i(m_j\theta + n_j\phi)] \\ &\quad - \exp[i(k\theta + l\phi)]\} \end{aligned} \quad (26)$$

Therefore, the displacement $W_{mn}(\xi)$ is obtained by substitution of Equation 20 into Equation 21. The strain $S_{mn}(\xi)$ is written by using $\tilde{W}(\xi, \theta, \phi)$ as

$$S_{mn}(\xi) = 1 + \left(\frac{1}{2\pi}\right)^2 \int_{-\pi}^{\pi} \int_{-\pi}^{\pi} \frac{\partial \tilde{W}}{\partial \xi} \times \exp[-i(m\theta + n\phi)] d\theta d\phi. \quad (27)$$

However, the unknown quantities W_j^0 and $Q_{m_j n_j}^{kl}$ are included in the solution of \tilde{W} (Equation 26). These values are obtained so that W_{mn} and S_{mn} satisfy the boundary conditions at the positions of the fibre breakages and on the matrix-

damaged regions, respectively. Considering Equations 6 and 17, the boundary conditions are expressed with \tilde{W} as

$$\left(\frac{1}{2\pi}\right)^2 \int_{-\pi}^{\pi} \int_{-\pi}^{\pi} \left[\frac{\partial \tilde{W}}{\partial \xi} \right]_{\xi=0} \times \exp[-i(m_j\theta + n_j\phi)] d\theta d\phi + 1 = 0 \quad (28)$$

$$Q_{m_j n_j}^{kl} = ||| |W_{kl} - W_{m_j n_j}| - Q ||| \text{sign}(W_{kl} - W_{mn}) \quad (29)$$

where

$$W_{m_j n_j} - W_{kl} = \left(\frac{1}{2\pi}\right)^2 \int_{-\pi}^{\pi} \int_{-\pi}^{\pi} \tilde{W} \{ \exp[-i(m_j\theta + n_j\phi)] - \exp[-i(k\theta + l\phi)] \} d\theta d\phi. \quad (30)$$

2.2. Probabilistic properties of fibre strength and expected number of fibre breakages

Fibre strength depends on the flaws in the fibre, that is, the fibre breaks at the flaw position when tensile strain exceeds a certain level which depends on the flaw size. The location and the size of the flaw in the fibre are probabilistic quantities. The probabilistic properties of the fibre strength can be obtained when those of the flaw are given. Now, we introduce an assumption that the existence of the flaws follows a Poisson process in space, that is,

1. The probability of the existence of the flaws does not depend on the existence of any other flaws.
2. The probability of the existence of more than one flaw in the same position can be neglected.

If the above assumptions are valid, the only quantity characterizing the probabilistic aspects of the fibre strength is the expected number $\mu_F(\epsilon)$ of the flaws breaking under a strain smaller than ϵ and existing in a unit-length fibre. The quantity $\mu_F(\epsilon)$ is determined from the probability distribution function $F(\epsilon|L)$ of the breaking strain of the fibre whose length is L . The probability that the fibre does not break under a strain ϵ is written as $1 - F(\epsilon|L)$. This probability is equal to the probability $\exp[-L\mu_F(\epsilon)]$ that no flaw breaking under ϵ exists in the fibre. Therefore, $\mu_F(\epsilon)$ is written as

$$\mu_F(\epsilon) = \ln[1 - F(\epsilon|L)]/L. \quad (31)$$

When the fibre breaking strain is ruled by a two-parameter Weibull distribution, $\mu_F(\epsilon)$ can be given

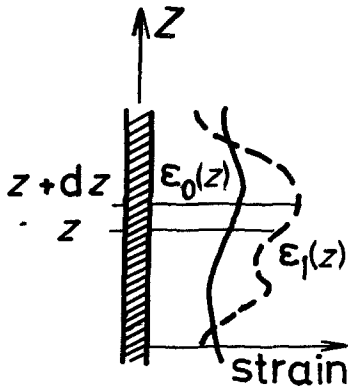


Figure 4 Change of the strain in the fibre.

in a power form of (ϵ/ϵ_L) as

$$\mu_F(\epsilon) = (\epsilon/\epsilon_L)^\gamma/L \quad (32)$$

where γ and ϵ_L are a shape parameter and a scale parameter, respectively.

When the strain in the fibre changes from $\epsilon_0(z)$ to $\epsilon_1(z)$ as shown in Fig. 4, the probability $P(\epsilon_1|\epsilon_0)$ that the fibre breaks in the region $[z_1, z_2]$ is obtained in the following way. In the infinitesimal region $[z, z + dz]$, the expected number $\mu_f(z) dz$ of the flaws breaking under above strain change is written as

$$\mu_f(z) dz = ||| \mu_F\{\epsilon_1(z)\} - \mu_F\{\epsilon_0(z)\} |||. \quad (33)$$

The expected number κ_f of such flaws existing in the region $[z_1, z_2]$ is given by the integration of Equation 33:

$$\kappa_f = \int_{z_1}^{z_2} \mu_f(z) dz = \int_{z_1}^{z_2} ||| \mu_F\{\epsilon_1(z)\} - \mu_F\{\epsilon_0(z)\} ||| dz. \quad (34)$$

When the breaking strain of the fibre follows Weibull distribution, Equation 34 is rewritten by using Equation 32 as

$$\kappa_f = \frac{1}{L} \int_{z_1}^{z_2} ||| \left(\frac{\epsilon_1(z)}{\epsilon_L} \right)^\gamma - \left(\frac{\epsilon_0(z)}{\epsilon_L} \right)^\gamma ||| dz. \quad (35)$$

As the flaw follows Poisson process, the probability P_S that no such flaw exists, in other words, that the fibre does not break, is written as

$$P_S(\epsilon_1|\epsilon_0) = \exp(-\kappa_f). \quad (36)$$

3. Numerical analysis

It is almost impossible to obtain the solution of general cases expressed in Section 2.1, so that the special cases that the fibres break at $\zeta = 0$ and the

matrix is damaged in the region $-\alpha < \zeta < \alpha$ around the broken fibres are solved.

In the case of a single broken fibre, equation of $W_0 (= W_j^0)$, $T(\zeta) (= T_{m_j n_j}^{kl}(\zeta) = W_{00}(\zeta) - W_{10}(\zeta))$ and $Q(\zeta) (= Q_{m_j n_j}^{kl}(\zeta))$ are lead from Equations 28, 29 and 30 as

$$W_0 = \left[1 + \int_0^\alpha B(s) Q(s) ds \right] / A \quad (37)$$

$$Q(\zeta) = T(\zeta) - \beta T(\alpha) \quad (38)$$

$$\sigma T(\zeta) = W_0 B(\zeta) + \int_{-\alpha}^\alpha C(\zeta - s) Q(s) ds \quad (39)$$

where

$$A = \left(\frac{1}{2\pi} \right)^2 \int_{-\pi}^\pi \int_{-\pi}^\pi \lambda d\theta d\phi$$

$$B(\zeta) = \left(\frac{1}{2\pi} \right)^2 \int_{-\pi}^\pi \int_{-\pi}^\pi \lambda^2 \exp(-\lambda|\zeta|) d\theta d\phi$$

$$C(\zeta) = \left(\frac{1}{2\pi} \right)^2 \int_{-\pi}^\pi \int_{-\pi}^\pi \frac{\lambda^3}{2} \exp(-\lambda|\zeta|) d\theta d\phi. \quad (40)$$

These integrals are executed numerically. The integrals for θ and ϕ are accomplished by a Gauss-integral method which has eight integral points in each direction. Equations 37, 38 and 39 are rewritten into simultaneous equations for W_0 , $Q_k (= Q(k\Delta s))$ and $T_k (= T(k\Delta s))$ by replacing the integrals in the above equations with a summation forms according to the numerical integral method.

When more than one fibre is broken, the external terms W_j^0 and $Q_{m_j n_j}^{kl}$ are calculated with an iteration method. The initial values are given by the use of the solution of one broken fibre case. The flow chart of this iteration process is indicated in Fig. 5. The parameters in Fig. 5 are

$$A_{jl} = \left(\frac{1}{2\pi} \right)^2 \int_{-\pi}^\pi \int_{-\pi}^\pi \lambda$$

$$\times \exp \{i[(m_l - m_j)\theta + (n_l - n_j)\phi]\} d\theta d\phi$$

$$B_{m_l n_l p q}^{m_j n_j}(\zeta) = G_{m_l - m_j, n_l - n_j}(\zeta) - G_{p - m_j, q - n_j}(\zeta)$$

$$C_{m_l n_l p q}^{m_j n_j ab}(\zeta) = H_{m_l - m_j, n_l - n_j}(\zeta) - H_{p - m_j, q - n_j}(\zeta)$$

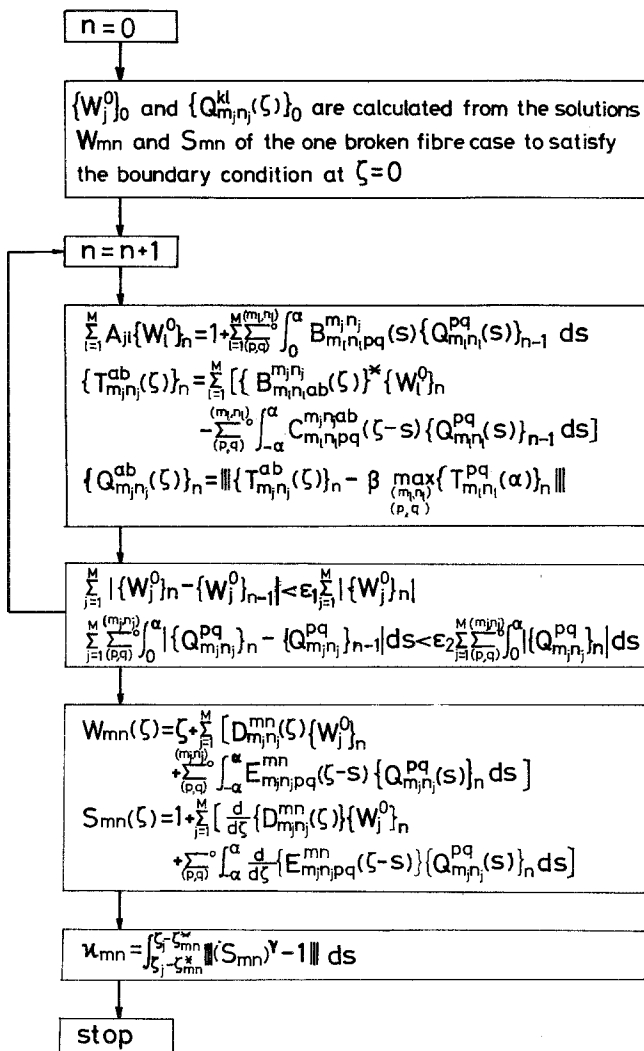
$$- H_{m_l - a, n_l - a}(\zeta) + H_{p - a, q - b}(\zeta)$$

$$D_{m_l n_l}^{mn}(\zeta) = G_{m_j - m, n_j - n}(\zeta)$$

$$E_{m_l n_l p q}^{mn}(\zeta) = H_{m_j - m, n_j - n}(\zeta) - H_{p - m, q - n}(\zeta)$$

(41)

Figure 5 Flow chart of the iteration process.



where

$$G_{mn}(\zeta) = \left(\frac{1}{2\pi}\right)^2 \int_{-\pi}^{\pi} \int_{-\pi}^{\pi} \exp[-\lambda|\zeta| + i(m\theta + n\phi)] d\theta d\phi$$

$$H_{mn}(\zeta) = \left(\frac{1}{2\pi}\right)^2 \int_{-\pi}^{\pi} \int_{-\pi}^{\pi} \frac{1}{2\lambda} \exp[-\lambda|\zeta| + i(m\theta + n\phi)] d\theta d\phi$$

In Equation 41, (m_j, n_j) and (m_i, n_i) mean those of the broken fibres. The values of 1×10^{-7} and 1×10^{-6} are taken as permissible errors ϵ_1 and ϵ_2 shown in Fig. 5, respectively, for present analysis. The difference is of the order of 10^{-4} in S_{mn} ($m, n \leq 4$) between two cases; the first is the case that the integral region $[-\pi, \pi] \times [-\pi, \pi]$ is divided into 4×4 and the other is the case that the region is divided into 2×2 regions. Therefore,

the latter (2×2 regions) is adopted because of computer time. The increment $\Delta s = 0.05$ is chosen in the present paper.

4. Numerical results and discussion

In the preceding sections the equations for this problem are obtained, neglecting the effects of transverse displacements. Solving these equations numerically, the nondimensional strain in the fibres and the nondimensional shear force between the neighbouring fibres are obtained. Then, the expected numbers of successive fibre breakages around the broken fibres are also calculated with the use of the strain in the fibre.

The nondimensional strains $S_{10}(\zeta)$ and $S_{11}(\zeta)$, and the nondimensional shear force $q_{00}^{10}(\zeta)$ are shown in Figs. 6, 7 and 8 when one fibre is broken at $m = n = \zeta = 0$. The case that the reaction force in the matrix-damaged region is assumed to be

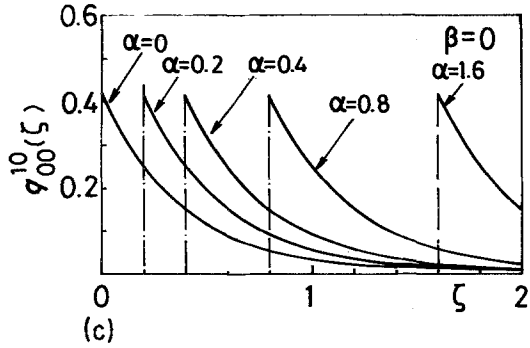
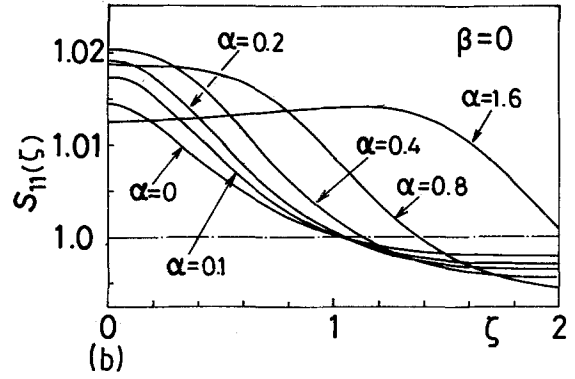
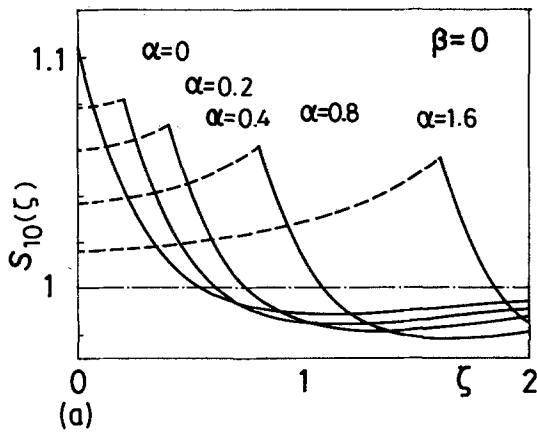


Figure 6 Nondimensional strains $S_{10}(\xi)$ and $S_{11}(\xi)$, and nondimensional shear force $q_{00}^{10}(\xi)$ for the case $\beta = 0$.

zero ($\beta = q/q_{\max} = 0$) is shown in Fig. 6. In Fig. 6a, $S_{10}(\xi)$ is shown as a function of ξ for various values of α . The maximum value of $S_{10}(\xi)$, which appears at $\xi = \alpha$, decreases with increasing α . In the region $\xi > \alpha$, $S_{10}(\xi)$ decreases rapidly, becomes smaller than 1 (that is, unloading regions appear) and gradually converges to 1. The coordinate ξ_{10}^* , where $S_{10}(\xi_{10}^*) = 1$, increases with α . $S_{11}(\xi)$ is shown in Fig. 6b. $|S_{11}(\xi) - 1|$ is much smaller than $|S_{10}(\xi) - 1|$. For small α , $S_{11}(\xi)$ gradually decreases even in the region $\xi < \alpha$. However, $S_{11}(\xi)$ increases in the region $\xi < 1.1$ for $\alpha = 1.6$. As α becomes larger, the maximum value of $S_{11}(\xi)$ increases for $\alpha < 0.4$, but decreases for $\alpha > 0.4$. The ratio between maximum strain changes in (1, 0) fibre and in (1, 1) fibre increases with α . The shear force $q_{00}^{10}(\xi)$ is shown in Fig. 6c. As $\beta = 0$ is assumed, $q_{00}^{10}(\xi) = 0$ where $\xi < \alpha$. Its maximum value is almost independent of α ($q_{00}^{10}(\alpha) \approx 0.42$).

In Fig. 7, $S_{10}(\xi)$, $S_{11}(\xi)$ and $q_{00}^{10}(\xi)$ for the case

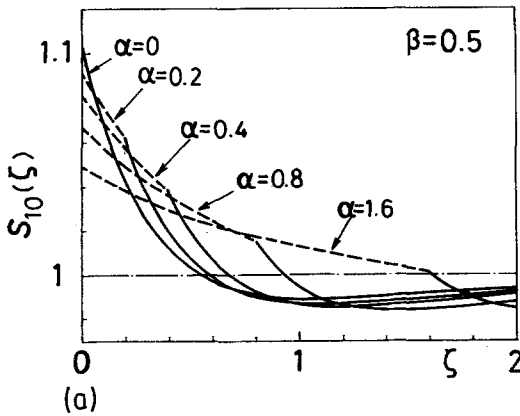
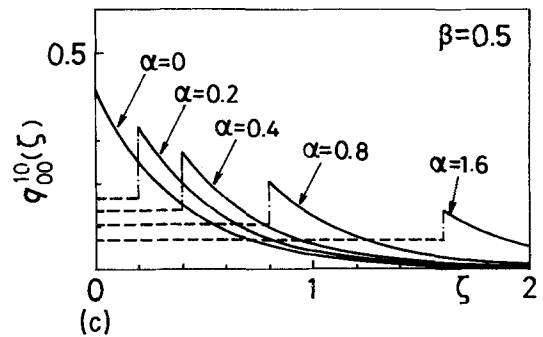
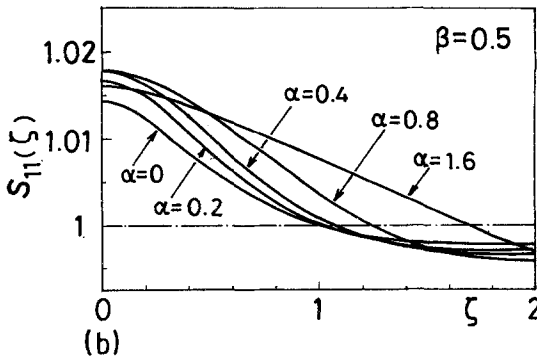


Figure 7 Nondimensional strains $S_{10}(\xi)$ and $S_{11}(\xi)$, and nondimensional shear force $q_{00}^{10}(\xi)$ for the case $\beta = 0.5$.



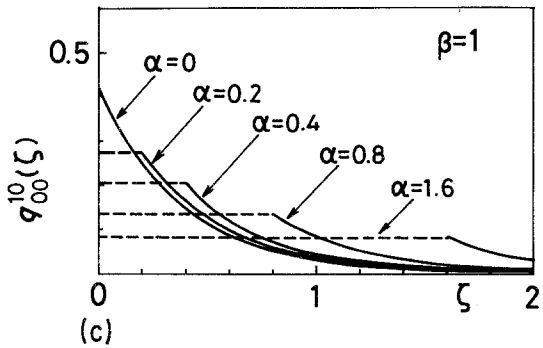
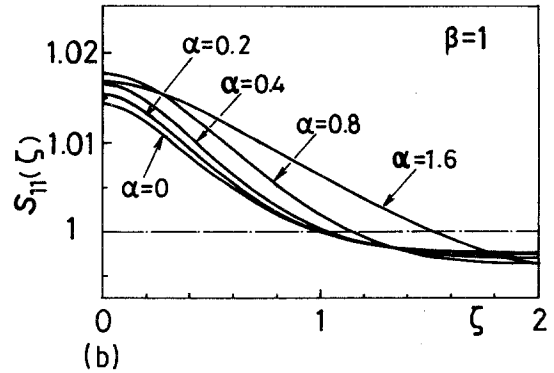
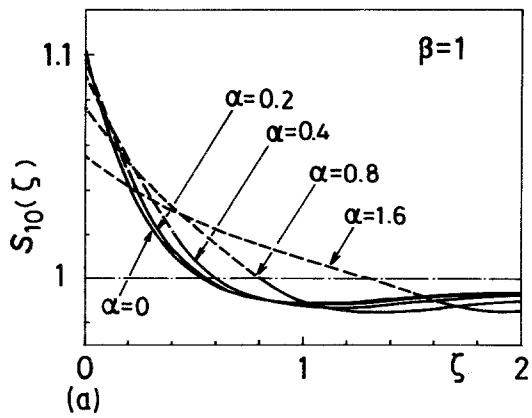


Figure 8 Nondimensional strains $S_{10}(\zeta)$ and $S_{11}(\zeta)$, and nondimensional shear force $q_{00}^{10}(\zeta)$ for the case $\beta = 1$.

$S_{10}(\zeta)$, $S_{11}(\zeta)$ and $q_{00}^{10}(\zeta)$ for the case $\beta = 1$ are shown in Fig. 8. These figures show similar trends to the case $\beta = 0.5$.

$S_{10}(0)$ and $S_{10}(\alpha)$ are shown in Fig. 9 as a function of α for $\beta = 0, 0.5$ and 1 . As mentioned above, $S_{10}(0)$ and $S_{10}(\alpha)$ (except $S_{10}(\alpha)$ for the case $\beta = 0$) decreases with increasing α . $S_{10}(0)$ increases with β , but on the contrary, $S_{10}(\alpha)$ decreases with increasing β . For $\beta = 0$, $S_{10}(\alpha)$ is greater than $S_{10}(0)$.

$\beta = 0.5$ are shown as a function of ζ for various values of α . The maximum of $S_{10}(\zeta)$ appears at $\zeta = 0$. $S_{10}(\zeta)$ decreases gradually with ζ where $\zeta < \alpha$. In the region $\zeta > \alpha$, $S_{10}(\zeta)$ rapidly decreases, becomes less than 1 and converges to 1 finally. $S_{11}(\zeta)$ has a tendency to decrease gradually in the region $\zeta < \alpha$ similar to $S_{10}(\zeta)$, and shows a trend similar to $S_{11}(\zeta)$ for the case $\beta = 0$. $q_{00}^{10}(\zeta)$ is also shown in Fig. 7c. It is noteworthy that the maximum of $q_{00}^{10}(\zeta)$, which appears at $\zeta = \alpha$, gradually decreases with increasing α . $q_{00}^{10}(\zeta)$ is $q_{\max}/2$ in the region $\zeta < \alpha$ because $\beta = 0.5$ is assumed.

q_{\max} is shown as a function of α in Fig. 10 for $\beta = 0, 0.5$ and 1 . As mentioned before, q_{\max} for the case $\beta = 0$ is almost independent of α . The greater β becomes, the faster q_{\max} decreases with increasing α . These results are very interesting and important because of the following reasons. If $\beta = 0$, the matrix-damaged regions spread infinitely when the load exceeds a certain level that the matrix failure arises. If $\beta \neq 0$, a value of α exists

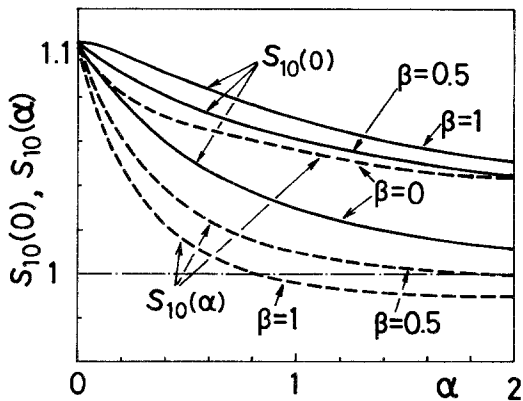


Figure 9 Nondimensional strains $S_{10}(0)$ and $S_{10}(\alpha)$ for $\beta = 0, 0.5$ and 1 .

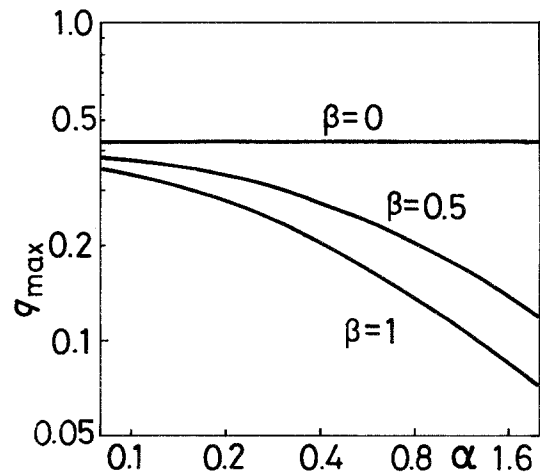


Figure 10 Maximum nondimensional shear force for $\beta = 0, 0.5$ and 1 .

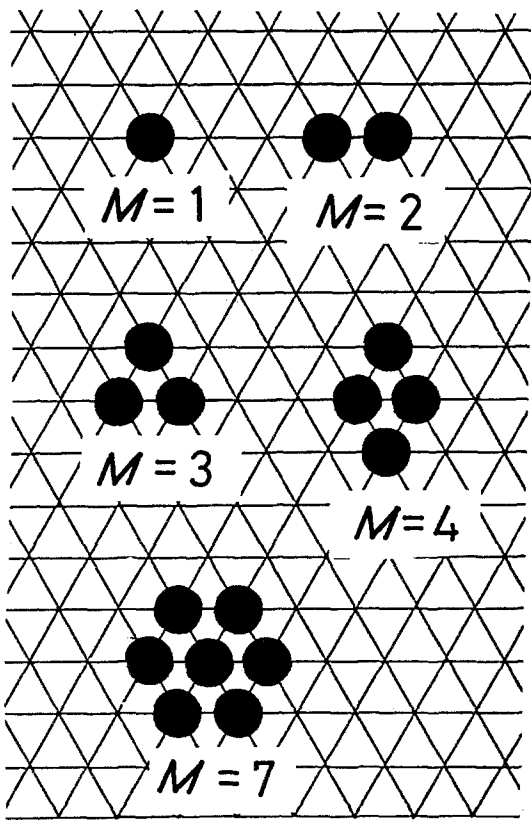


Figure 11 Broken patterns of fibre.

corresponding to the external force. If the load is set constant (that is, q_{\max} is set fixed), α for the case $\beta = 0.5$ is greater than that for the case $\beta = 1$.

Results are obtained when more than one fibres are broken neighbouring each other. However, the results for the case $\beta = 0$ are unrealistic and those for the case $\beta = 1$ possesses the trends similar to those for $\beta = 0.5$, so that only the results for $\beta = 0.5$ are shown hereafter. The broken patterns calculated are shown in Fig. 11. The value q_{\max} is plotted in Fig. 12 as a function of M (number of the fibres broken adjacent to each other) for various α . It increases with M . This phenomenon means that the matrix-damaged regions spread noticeably as the flaw size grows. Furthermore, the chance that the broken fibres are linked to each other increases with the flaw size M . The value q_{\max} is also shown as a function of α for several flaw sizes M in Fig. 13. It decreases with increasing α for $M > 1$, too.

The expected number κ_{mn} of successive fibre breakages around a broken fibre is shown in Fig. 14 as a function of α for $\beta = 0.5$. The shape parameter γ of the fibre strength is assumed to

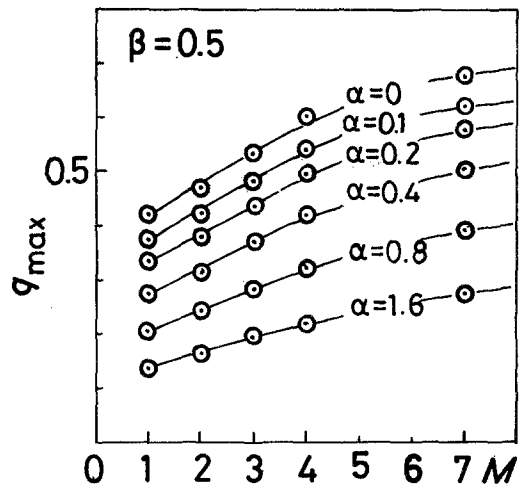


Figure 12 Maximum nondimensional shear force as a function of flaw size M for various α .

be 5 in the present analysis. This value is reasonable for glass or carbon fibre. At first, κ_{10} increases with α , but begins to decrease at $\alpha \approx 1$ because of the combining effects of decreasing maximum strain and increasing the size ξ_{10}^* of the region of increased strain. The displacement W_0 where a fibre is broken is also shown with a chain line in this figure. W_0 increases in proportion to α . This phenomenon is very important because the strain in the fibre apart from the broken one is proportional to W_0 . Therefore, κ_{mn} increases almost in proportion to α , when the fibre locates distant from the broken one.

The expected number $\sum_M^0 \kappa_{mn}$ of successive fibre breakages occurring in the surrounding fibres is shown in Fig. 15 for several values of α . It

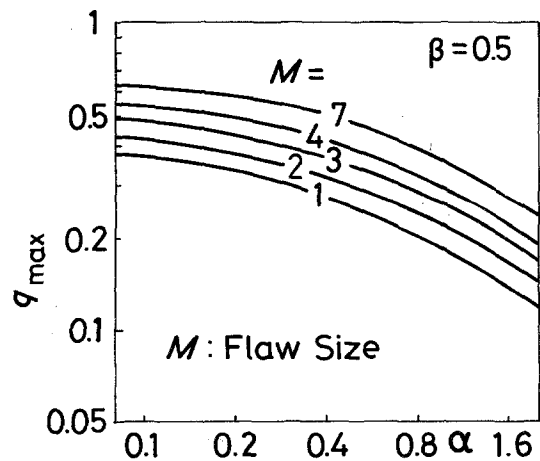


Figure 13 Maximum nondimensional shear force as a function of α for various flaw sizes.

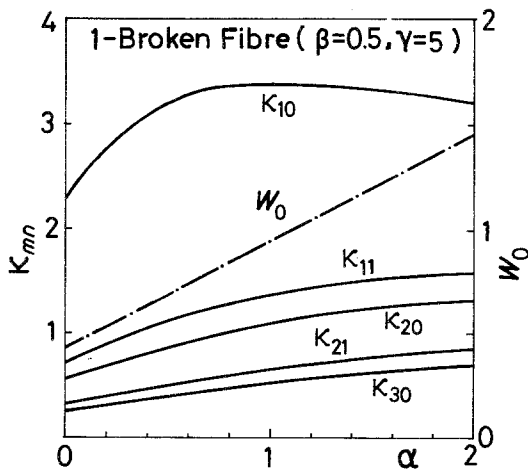


Figure 14 The expected number κ_{mn} of successive fibre breakages for one broken fibre and the displacement W_0 of the (0, 0) fibre at $\zeta = 0$.

increases faster than M , and is approximated as

$$\sum_M^0 \kappa_{mn} \approx C_M M^k \quad (42)$$

C_M and $k (> 1)$ are constants. This means that the probability, that a flaw grows, increases with the flaw size.

5. Conclusions

The strain in the fibres around the broken fibres with matrix failure is calculated based on a

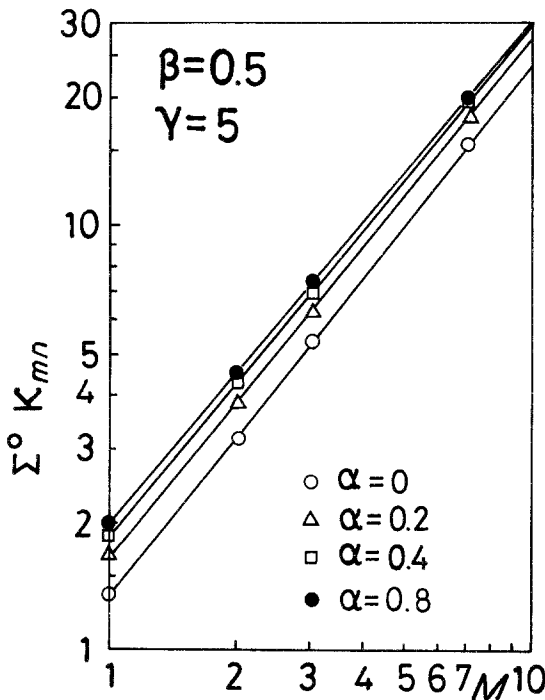


Figure 15 The expected number $\sum_M^0 \kappa_{mn}$ of successive fibre breakages as a function of flaw size M for various α .

hexagonal-array shear-lag model, and the expected number κ_{mn} of successive fibre breakages is obtained with the assumption that the flaws in the fibre follow a Poisson process. From these analytical results, the following conclusions are obtained.

1. The strains ($S_{10}(0)$ and $S_{10}(\alpha)$) decrease when the size α of the matrix-damaged region becomes larger except $S_{10}(\alpha)$ for the case $\beta = 0$.

2. Strain increasing region extends noticeably as α becomes larger.

3. For the case $\beta = 0$, the maximum shear force q_{\max} is almost independent of α . It means that the matrix failure progresses infinitely. However, for the case $\beta \neq 0$, q_{\max} decreases with increasing α . It means that a size of the matrix-damaged region can be obtained uniquely if an external force is given.

4. The maximum shear force q_{\max} increases with flaw size M .

5. The expected number κ_{mn} of the fibre breakages apart from the broken fibre increases in proportion to the displacement W_0 at $m = n = \zeta = 0$.

6. If the size α is small, the expected number $\sum_M^0 \kappa_{mn}$ around the broken fibres increase with α . However, if the size α becomes large, $\sum_M^0 \kappa_{mn}$ begins to decrease due to the decreases of the maximum strains.

7. $\sum_M^0 \kappa_{mn}$ increases rapidly when the flaw size M becomes larger. It means that there is a critical flaw size that the probability of the fracture can not be neglected.

The results obtained in the present paper can be basic data for the calculation of practical probabilistic quantities of the strength of the composite materials. The practical probabilistic quantities, that is, asymptotic formula of the probability distribution function, of the fracture strain will be calculated in a coming paper.

Acknowledgement

The author wishes to express his gratitude to Professor Akira Kobayashi for his kind advices and encouragements and to Dr Nobuo Takeda for his kind advice, both with the Interdisciplinary Research, Faculty of Engineering, University of Tokyo. This work is partly supported by the Sakkokai Foundation.

Appendix: Homogeneous and orthotropic model

A strain around broken fibres is also obtained with the assumption that composite materials are

homogeneous and orthotropic. When the transverse displacements are neglected, an equilibrium equation is written with the use of an axial displacement w as

$$G_{LT} \left(\frac{\partial^2 w}{\partial x^2} + \frac{\partial^2 w}{\partial y^2} \right) + E_L \frac{d^2 w}{dz^2} = f(x, y, z). \quad (A1)$$

The function $f(x, y, z)$ in the right-hand side is induced by the defects in the composite. Equation A1 is rewritten in a nondimensional form as

$$\frac{\partial^2 W}{\partial \xi^2} + \frac{\partial^2 W}{\partial \eta^2} + \frac{\partial^2 W}{\partial \zeta^2} = F(\xi, \eta, \zeta) \quad (A2)$$

$$W = \left\{ \frac{1}{r_0 \epsilon_\infty} \left(\frac{G_{LT}}{E_L} \right)^{1/2} \right\} w \quad (A3)$$

$$\xi = \frac{x}{r_0}, \quad \eta = \frac{y}{r_0}, \quad \zeta = \frac{z}{r_0} \left(\frac{G_{LT}}{E_L} \right)^{1/2} \quad (A4)$$

where $\pi r_0^2 = A_E$. When matrix failures occur in the region around the broken fibres, $F(\xi, \eta, \zeta)$ is written as

$$F(\xi, \eta, \zeta) = \sum_{j=1}^N \left[W_j(\xi, \eta) U(1 - \rho) \frac{\partial}{\partial \zeta} \{ \delta(\zeta - \zeta_j) \} + \Theta_j(\xi, \eta, \zeta) U(\alpha_j - |\zeta - \zeta_j|) \frac{\partial}{\partial \rho} \{ \delta(\rho - 1) \} \right] \quad (A5)$$

$$W_j(\xi, \eta) = \frac{1}{2} \lim_{\Delta \rightarrow 0} [W(\xi, \eta, \zeta + \Delta) - W(\xi, \eta, \zeta - \Delta)] \quad (A6)$$

$$\Theta_j(\xi, \eta, \zeta) = \frac{1}{2} \lim_{\Delta \rightarrow 0} \{ W(\rho + \Delta, \theta, \phi) - W(\rho - \Delta, \theta, \phi) \} \quad (A7)$$

$$\rho^2 = (\xi - \xi_j)^2 + (\eta - \eta_j)^2, \quad \tan \theta = \eta/\xi$$

Application of the theory of Green's function gives the solution of Equation A2 as

$$W = \frac{1}{4\pi} \iiint_V F(\xi', \eta', \zeta') \frac{1}{R} d\xi' d\eta' d\zeta'$$

*

$$\int_{-\pi}^{\pi} \left[\frac{\rho \cos(\theta - \theta') - \rho'}{R^5} \right]_{\rho'=1}^{\rho} = 2 \int_0^{\pi/2} \frac{4\rho^2 \cos^2 \theta \sum_{i=0}^4 R_1^i R_2^{4-i} - (R_1 + R_2)(R_1^5 + R_2^5)}{R_1^5 R_2^5 (R_1 + R_2)} d\theta \sim kR^{-5}$$

where

$$R_1 = [1 + \rho^2 + 2\rho \cos \theta + (\zeta - \zeta')^2]^{1/2}, \quad R_2 = [1 + \rho^2 - 2\rho \cos \theta + (\zeta - \zeta')^2]^{1/2}.$$

$$= \frac{1}{4\pi} \sum_{j=1}^N \left\{ \iint_{\rho' < 1} W_j(\rho', \theta') \right.$$

$$\times \left[\frac{\zeta - \zeta'}{R^3} \right]_{\zeta'=\zeta_j}^{\zeta} \rho' d\rho' d\theta' + \int_{|\zeta - \zeta_j| < \alpha_j} \int_{-\pi}^{\pi} \Theta_j(\zeta', \theta') \times \left[\frac{\rho \cos(\theta - \theta') - \rho'}{R^3} \right]_{\rho'=1}^{\rho} d\theta' d\zeta' \quad (A8)$$

$$R^2 = \rho^2 + \rho'^2 - 2\rho\rho' \cos(\theta - \theta') + (\zeta - \zeta')^2$$

The differentiation of W by ζ gives a nondimensional strain as

$$S = \frac{dW}{d\zeta} = \frac{1}{4\pi} \sum_{j=1}^N \left\{ \iint_{\rho' < 1} W_j(\rho', \theta') \right.$$

$$\times \left[\frac{R^2 - 3(\zeta - \zeta_j)^2}{R^5} \right]_{\zeta'=\zeta_j}^{\zeta} \rho' d\rho' d\theta'$$

$$+ \int_{|\zeta - \zeta_j| < \alpha_j} \int_{-\pi}^{\pi} \Theta_j(\zeta', \theta')$$

$$\times \left[\frac{3\{\rho \cos(\theta - \theta') - \rho'\}(\zeta - \zeta')}{R^5} \right]_{\rho'=1}^{\rho} d\theta' d\zeta' \quad (A9)$$

The first term of S decreases in proportion to R^{-3} , and the second term decreases in proportion to R^{-5} when $|\zeta - \zeta_j|$ is not large,* so that strain can be approximated with the first term alone when R is not small.

References

1. H. SUEMASU, *Trans. Jpn. Soc. Compos. Mater.* 8 (1983) 1.
2. B. W. ROSEN, *AIAA J.* 2 (1964) 1985.
3. C. ZWEBEN, *ibid.* 6 (1968) 2325.
4. J. G. GOREE, L. R. DHARANI and W. F. JONES, NASA, CR, 3453 (1981).
5. J. M. HEDGEPEETH and P. V. DYKE, *J. Compos. Mater.* 1 (1967) 294.

Received 7 March

and accepted 15 June 1983